RESEARCH ARTICLE

Check for updates

Heteroanionic [VOxS4−x] groups: tetrahedral units with large birefringence for mid-infrared nonlinear optical crystals†

Shengzi Zhang,‡[a,b] Linfeng Dong, [ID] ‡[a,d] Bohui Xu, [ID] [a,d] Huige Chen,[a,d] Hao Huo,[a,d] Fei Liang, [ID] [a] Rui Wu,[c] Pifu Gong [ID] *[a] and Zheshuai Lin [ID] *[a,d]

Tetrahedral groups can possess a wide bandgap and large second harmonic generation (SHG) response in nonlinear optical (NLO) materials; however, they usually exhibit a small optical birefringence owing to the low structural anisotropy, which would deteriorate the NLO performance. Herein, the $[VO_xS_{4-x}]$ ($x = 0-4$) tetrahedra that combine the V^{5+} cation with oxygen−sulfur hybrid anions are highlighted as a type of good structural group to overcome the above problem. Using theoretical calculations, we systematically investigate the optical and NLO properties of all reported V^{5+}-based thiovanadates. The calculated results reveal the largest birefringence (~0.37 in $Ba_5V_2O_4S_8$) among the pure tetrahedron-based compounds and indicate the potential of $[VO_xS_{4-x}]$ units in enhancing the birefringence and well-balanced NLO performance suitable for the mid-infrared (mid-IR) region. Furthermore, Na_3VOS_3 in this family is selected for experimental synthesis and measurements to verify our strategy and calculations. This work demonstrates that the $[VO_xS_{4-x}]$ ($x = 0-4$) tetrahedral groups, which had been overlooked for a long time, are a good type of birefringent and NLO unit for the exploration of mid-IR NLO materials.

Introduction

Mid-infrared (mid-IR) nonlinear optical (NLO) crystals are the key components in all-solid-state infrared tunable lasers, and they can convert the laser radiation from the common near-IR spectral region (*e.g.*, Nd:YAG laser @ 1064 nm) to the mid-IR regions.[1–4] This significantly expands the laser application range in many civil and military fields such as medical imaging, laser displays, remote communications, and environmental monitoring.[5–13] To reach the practical applications, a mid-IR crystal should satisfy the high-performance criteria including[14,15] (i) a wide IR transparency covering the atmospheric windows, (ii) large NLO coefficient d_{eff} for high conversion efficiency, (iii) wide band gap to achieve a high laser-induced damage threshold (LDT) during the high power laser input, (iv) sufficient birefringence for IR phase-matching and

aFunctional Crystals Lab, Technical Institute of Physics and Chemistry, Chinese Academy of Sciences, Beijing 100190, China. E-mail: zslin@mail.ipc.ac.cn
bNational Institute of Metrology, Beijing 100029, China
cBeijing Academy of Quantum Information Sciences, Beijing 100193, China
dCenter of Materials Science and Optoelectronics Engineering, University of Chinese Academy of Sciences, Beijing 100049, China
†Electronic supplementary information (ESI) available: Experimental procedures, crystal structure data, photoluminescence spectroscopy, Raman spectra. CCDC 2366824. For ESI and crystallographic data in CIF or other electronic format see DOI: https://doi.org/10.1039/d4qi01442a
‡These authors contributed equally.

(v) good crystal growth habit and chemical stability. Up to now, only AgGaS₂ (AGS),[16] AgGaSe₂,[17] and ZnGeP₂ [18] are commercially available; however, these crystals all have their own drawbacks such as low LDT in AGS and strong two-photon absorption in ZnGeP₂ pumping using Nd:YAG lasers. Therefore, it is urgent to explore novel mid-IR NLO crystals with well-balanced performance.

After extensive efforts for decades, dozens of promising mid-IR NLO candidates such as $BaGa_4Se_7$, $LiGaS_2$, $LiInS_2$, $CdSiP_2$, $AMgAgGa_6S_{11}$ (A = K, Rb), $BaZnGeS_4$, Zn_2NX (X = Cl, Br), $Li_2K_4TiOGe_4O_{12}$, $KYGeS_4$, and $Hg_7P_2Se_{12}$ have been reported.[19–28] Through systematic structure–property analysis, the tetrahedral units were highlighted as good IR NLO-active "material genes" to realize the balance between the large NLO coefficients and wide band gaps.[29,30] In addition, the polar arrangement of these tetrahedral units, *e.g.*, in the diamond-like structures, would result in a tightly packed framework with the tetrahedra pointing in a special crystallographic axis, which is conducive to the large NLO effects.[31–37] However, the birefringence of the tetrahedron-based NLO crystals are usually rather small with the value ranging from 0.01 to 0.03. Such small optical birefringence can be attributed to the low structural anisotropy of the tetrahedral groups. Thus, it is urgent and necessary to improve the birefringence while keeping the balanced NLO performance in tetrahedron-based NLO crystals.

Normally, the birefringence of a crystal is positively related to the polarization anisotropy of its microscopic units. One

could reach a large birefringence by increasing the polarization anisotropy. Introducing distorted polyhedra with d^0 cations has been proven to be an efficient way to improve the polarization anisotropy and birefringence, and the degree of distortion generally follows the order $V^{5+} > W^{6+} > Ti^{4+} > Nb^{5+} > Ta^{5+} > Zr^{4+}$.[38] Thus, polyhedra containing the V^{5+} ion are likely to produce a large birefringence. For instance, $NaCa_4V_5O_{17}$ with $[V_2O_7]$ units and $[V_3O_{10}]$ units exhibits a large birefringence of about 0.1 at 1064 nm,[39] and YVO_4 with $[VO_4]$ tetrahedra possesses an ultra-large birefringence of 0.225 at 633 nm.[40] Therefore, V^{5+} cations can be regarded as good central cations to improve the birefringence of tetrahedron-based NLO crystals.

Constructing heteroanionic tetrahedra by coordinating with different electronegative ligands is also an efficient way to enhance the structural anisotropy for a large birefringence. In a recent review, Chen *et al.* investigated typical and emerging compounds, and demonstrated that the presence of an anisotropic structure building unit that encompasses diverse chemical bonds (ABUCB) in DUV/UV NLO compounds contributes to an increase in birefringence.[41] For example, Pan *et al.* introduced the $[PO_3F]$ unit into phosphates, and realized a large birefringence of 0.03 @ 1064 nm and 0.05 @ 589.3 nm in $(NH_4)_2PO_3F$ [42] and $NaNH_4PO_3F·H_2O$, respectively.[43] Ye *et al.* tuned the ligands of $[SO_4]$ units, and achieved a large birefringence in $C(NH_2)_3SO_3F$ [44] with $[SO_3F]$ and $M(SO_3NH_2)_2$ (M = Sr, Ba) with $[SO_3NH_2]$.[45] Our group also realized a large birefringence in $CsSO_3CF_3$ by constructing the heteroanionic $[SO_3CF_3]$ unit.[46] Very recently, oxychalcogenides with heteroanionic units were developed to be promising IR NLO materials. The heteroanionic tetrahedral groups, *e.g.*, $[PO_3S]$ unit in Na_3PO_3S,[47] $[SbOS_4]$ unit in $Sr_6Cd_2Sb_6O_7S_{10}$,[48] and $[GeO_2Se_2]$ unit in $BaGeOSe_2$,[49] with a large structural anisotropy can possess enhanced hyperpolarizability and polarization anisotropy, which would result in large NLO effects and birefringence in the mid-IR region.

To improve the birefringence while keep the balanced NLO performance of the tetrahedral NLO chalcogenides, we propose to combine the above-mentioned two material design strategies. In this work, the V^{5+} cation is chosen as the tetrahedrally coordinated cation, and heteroanions (O^{2-} and S^{2-}) are used as the ligands, thus forming the thiovanadates containing $[VO_xS_{4-x}]$ ($x = 0–4$) groups (Fig. 1a). It should be noted that the linear and NLO properties in the $[V–O–S]$ system were overlooked for a long time, and there has been no systematic research on this series yet. Our first-principles calculations show that the $[V–O–S]$ series of compounds, not only with the $[VO_xS_{4-x}]$ tetrahedra, but also with other types of $[V–O–S]$ polyhedra, possess a large birefringence, verifying the validity of our strategy. The birefringence record of the pure tetrahedron-based compounds was found to be about 0.37 in $Ba_5V_2O_4S_8$. Furthermore, $β-Na_3VOS_3$ containing the $[VO_xS_{4-x}]$ tetrahedra was selected for further experimental verification. In addition, materials design and structure–property correlation analysis based on $β-Na_3VOS_3$ were carried out. It is concluded that the $[VO_xS_{4-x}]$ ($x = 0–4$) tetrahedral groups are a type of NLO unit with good birefringence in the mid-IR NLO materials.
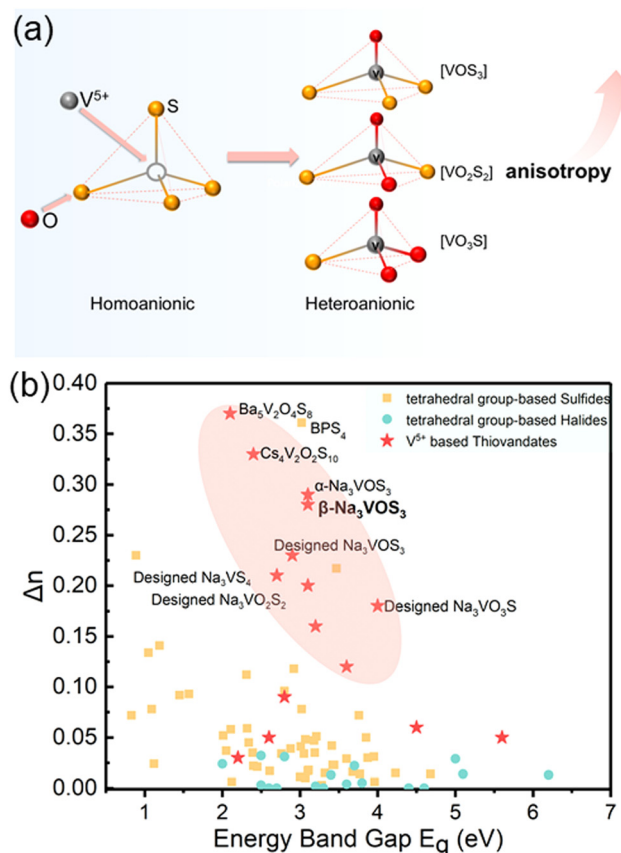
Fig. 1 (a) Schematic of our design strategy for enlarging the birefringence of the tetrahedral group; (b) balanced performance coordinate of the $Δn$ and energy band gap in the tetrahedral-based sulfides, halides and V^{5+}-based thiovanadates (the data of the tetrahedral-based sulfides and halides are from ref. 33 and 50, and compounds are listed in Table S1†).

Results and discussion

Although vanadates are widely used as important optoelectronic functional materials in such fields as photocatalysis, nonlinear optics, and solar energy utilization,[51–53] their thio-derivatives, *i.e.*, thiovanadate, have not been extensively studied yet. Our survey in the Inorganic Crystal Structure Database (ICSD, version 5.1.0) shows that there only exist ten V^{5+}-based thiovanadates from experimental studies. Their main structural features, including the microscopic structural groups, are listed in Table 1. Clearly, most of the reported thiovanadates consist of $[VO_xS_{4-x}]$ tetrahedra, except $Cs_5V_3O_3S_{15}$ and $Cs_4V_2O_2S_{10}$, which contain $[VOS_5]$ octahedra. By the self-consistent *ab initio* approach, the band gaps E_g, birefringence $Δn$ and NLO coefficients d_{ij} of these thiovanadates are investigated for the first time, although their structures have been known for decades. The calculated birefringence of the selected thiovanadates is displayed in Fig. 1b. Compared with traditional tetrahedral sulfides and halides, it is clear that the birefringence values of the V^{5+}-based thiovanadates are much larger, as shown in the pink field. Notably, the new birefrin-

Research Article

Table 1 Calculated linear and nonlinear optical properties of the V^{5+}-based thiovanadates. CS: centrosymmetric, NCS: non-centrosymmetric. Experimental values are shown in brackets

Compounds	Space groups	Groups	CS/NCS	E_g (eV)	Δn @ 1 μm	d_{ij} (pm V^{-1})	ICSD no.
$Cs_5V_3O_3S_{15}$	$P2_1/c$	$[VOS_5]$	CS	2.6	0.05	—	280814
$Cs_4V_2O_2S_{10}$	$P2_1/n$	$[VOS_5]$	CS	2.4	0.33	—	280815
$Ba_5V_2O_4S_8$	$Cmce$	$[VO_2S_2]$	CS	2.1 (2.2 [55])	0.37	—	18731
$Ba_{10}V_6O_{18}S_7$	$P6_3$	$[VO_3S]$	NCS	2.2 (2.2 [56])	0.03	$d_{33} = 4.2$	235360
$Ba_6V_4O_5S_{11}$	$Pnma$	$[VS_4], [VOS_3], [VO_2S_2]$	CS	2.8	0.09	—	59294
$K_3VO_2S_2$	$P2_1/c$	$[VO_2S_2]$	CS	3.6	0.12	—	419398
K_3VO_3S	$P2_1/m$	$[VO_3S]$	CS	4.5	0.06	—	419400
$Na_3VO_2S_2$	$Pbca$	$[VO_2S_2]$	CS	3.1	0.20	—	174237
Na_3VOS_3 (α-phase)	$Pnma$	$[VOS_3]$	CS	3.1	0.29	—	415218
Na_3VOS_3 (β-phase)	$Cmc2_1$	$[VOS_3]$	NCS	3.1	0.28	$d_{15} = 10.6$	415217
Designed Na_3VS_4	$Cmc2_1$	$[VS_4]$	NCS	2.7	0.21	$d_{33} = 53.5$	This work
Designed Na_3VOS_3	$Cmc2_1$	$[VOS_3]$	NCS	2.9	0.23	$d_{33} = 22.9$	This work
Designed $Na_3VO_2S_2$	$Cmc2_1$	$[VO_2S_2]$	NCS	3.2	0.16	$d_{33} = 17.3$	This work
Designed Na_3VO_3S	$Cmc2_1$	$[VO_3S]$	NCS	4.0	0.18	$d_{33} = 18.3$	This work
Designed Na_3VO_4	$Cmc2_1$	$[VO_4]$	NCS	5.6	0.05	$d_{33} = 5.4$	This work

gence record of the pure tetrahedron-based compounds is improved to 0.37 in $Ba_5V_2O_4S_8$ and it verifies our birefringence enhancing strategy (for the refractive indices for all compounds, see Table S1†).

At the same time, the band gaps of the thiovanadates are evaluated by hybrid sx-LDA functionals, whose results match well with the available experimental values and the previous research studies.[29,33,54] As shown, the alkali metal thiovanadates exhibit wide band gaps, some of which can even exceed 3.0 eV and are favorable for high LDT. In all known thiovanadates, there are only two non-centrosymmetric compounds containing $[VO_xS_{4-x}]$ groups, *i.e.*, $Ba_{10}V_6O_{18}S_7$ with the space group $P6_3$ and Na_3VOS_3 with $Cmc2_1$ (β-phase), whose SHG potentials were neglected for a long time. By the theoretical investigation, their NLO properties are firstly studied. Remarkably, the latter compound has large SHG coefficients with the largest component of 10.6 pm V^{-1}, making it a promising crystal for mid-IR NLO applications. For this reason, we further investigated its NLO origin and performed experimental verification.

The single crystals of β-Na_3VOS_3 were obtained by traditional high-temperature solid-state reaction, and its structure was resolved by single crystal X-ray diffraction (CCDC no. 2366824†). Related structural information, including the structural refinement information, are summarized in Tables S2–S4.† The resolved crystal structure is in good agreement with that reported by Schnabel *et al.*[57] β-Na_3VOS_3 belongs to the non-centrosymmetric space group $Cmc2_1$, and its structure is shown in Fig. 2a with cell parameters a = 9.5667(7) Å, b = 11.8659(9)(2) Å, c = 5.8806(4) Å, with $\alpha = \beta = \gamma = 90°$ and Z = 6. This structure contains two Na atoms, one V atom, one O atom, and two S atoms in the symmetric unit. All of the V atoms are tetra-coordinated with three S atoms and one O atom to form the $[VOS_3]$ tetrahedra. The V–O bond length is 1.673 Å, while the V–S bond lengths vary from 2.175 to 2.197 Å. The S–V–S/O bond angles range from 109.97° to 115.16°. The large structural distortion in the $[VOS_3]$ tetrahedra would result in a large microscopic polarization anisotropy.

In addition, all of these tetrahedra are distributed discretely in the lattice, and exhibit a relatively ordered arrangement with the O atoms pointing along the c-axis. Such a polarity-enhanced arrangement is favorable for realizing a large NLO response and birefringence, which will be further analyzed below. The two crystallographically independent Na^+ cations are inserted in the space between the $[VOS_3]$ tetrahedra to balance the charge, and they are surrounded by the neighboring S and O atoms. The distance between Na and S/O ranges from 2.283 Å to 3.212 Å. Each oxygen atom connects to three Na^+ and one V^{5+} cations, with the V–O–V angles varying from 106.09° to 119.48°. Detailed crystal data, including the fractional atomic coordinates, isotropic/anisotropic displacement parameters, and bond lengths are listed in Tables S2–S5.†

The calculated electronic band structure and partial density of states (PDOS) in β-Na_3VOS_3 are shown in Fig. 2b. The band structure indicates that β-Na_3VOS_3 is an indirect bandgap semiconductor with a band gap of 3.1 eV. As PDOS shows, the top of the valence band (VB) is primarily occupied by S-3p and O-2p orbitals, while the bottom of the conduction band (CB) has contributions from the V-3d and S-3p orbitals. Both parts of the orbitals exhibit significant dispersion, indicating the strong hybridization between V and O/S in the $[VOS_3]$ tetrahedra. Meanwhile, the VB maximum and CB minimum, *i.e.*, the highest occupied molecular orbitals (HOMO) and the lowest unoccupied molecular orbitals (LUMO), predominantly have contributions from the p-orbitals of S and d-orbitals of V, as shown in Fig. 2d. As the optical properties are mainly dependent on the electronic transition between the top of VB and the bottom of CB, the $[VOS_3]$ tetrahedra determine the optical properties of the title compound. In addition, the refractive index dispersion (displayed in Fig. 2c) reveals that β-Na_3VOS_3 is a biaxial crystal, and it possesses a very large birefringence of 0.28 at 1064 nm.

Since β-Na_3VOS_3 crystallizes in the $mm2$ point group, under the Kleinman's symmetry constraints, there are three independent SHG coefficients; they are calculated to be $d_{15} = -10.6$ pm
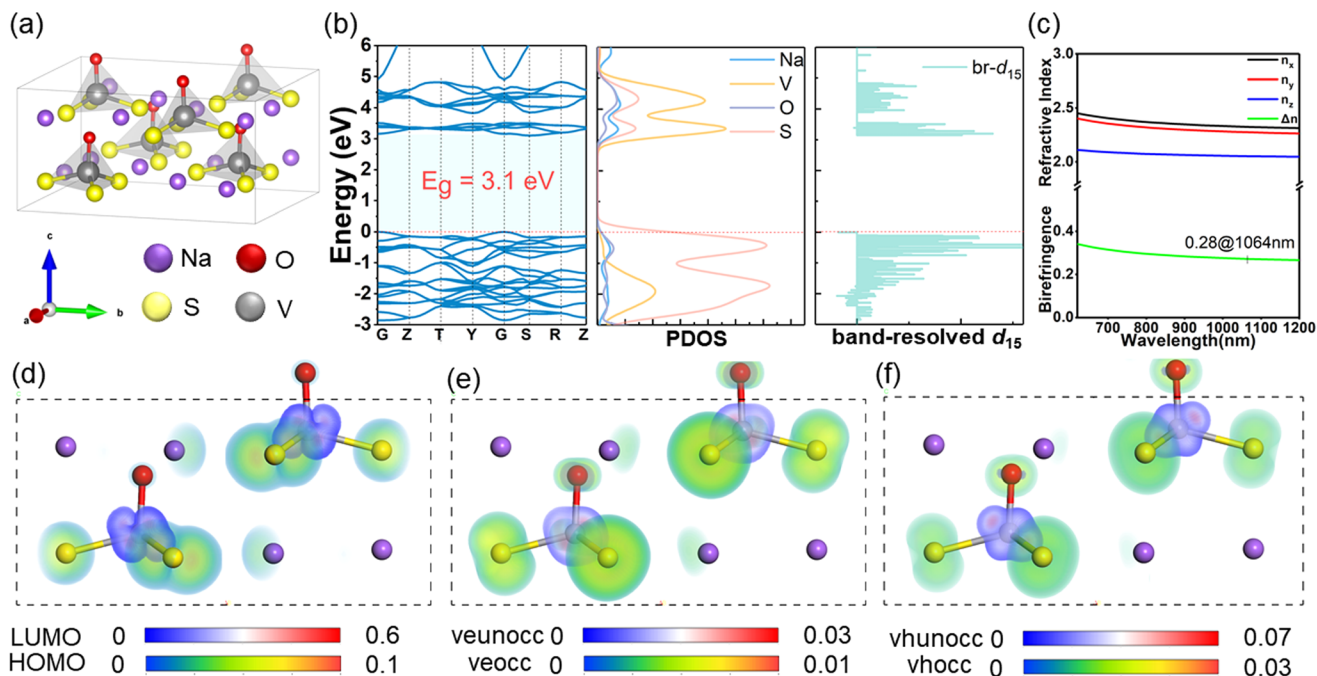
Fig. 2 (a) Unit cell in β-Na₃VOS₃; (b) band structures (left panel), PDOS (middle panel) and band-resolved d_{15} (right panel); (c) dispersion curves of the refractive indices and birefringence of β-Na₃VOS₃; (d) HOMO and LUMO; SHG-weighted density for occupied and unoccupied (e) VE process; (f) VH process.

V^{-1}, d_{24} = 8.3 pm V^{-1}, and d_{33} = 4.2 pm V^{-1}. To further analyze the origin of such strong NLO effect, the band-resolved d_{15}, the largest SHG coefficient, was plotted and is shown in Fig. 2b. Clearly, the orbitals at the top VB and the CB bottom play predominant roles in determining the SHG responses. In order to clearly exhibit the contribution from the orbitals in real-space, the SHG-weighted densities of the virtual electron (VE) process and virtual hole (VH) process for d_{15} are plotted in Fig. 2e and f, respectively. As expected, the large NLO effect of β-Na₃VOS₃ mainly originates from the large microscopic second-order polarization of the [VOS₃] tetrahedral, as well as their polarization superposition arrangement, while that from the Na$^+$ ions can be neglected.

To verify the good NLO performance of β-Na₃VOS₃, we synthesized its polycrystalline powders and carried out the measurements. The X-ray diffraction patterns of the obtained powders agree well with the calculated diffraction patterns, indicating the high purity of the compound that we obtained (as shown in Fig. 3a). The UV-vis-NIR diffuse reflectance spectrum in Fig. 3b shows that the optical band gap of β-Na₃VOS₃ is about 2.1 eV, slightly lower than the theoretical value. This might be attributed to some impurities presented in the sample. The powder SHG measurements based on the Kurtz–Perry method[58] was carried out to investigate the NLO effects of β-Na₃VOS₃. Fig. 3c and d show the SHG responses of β-Na₃VOS₃ (and benchmark AgGaS₂), and they increase gradually with the increase of the particle sizes, indicating the phase matching ability of this compound. In the particle size range of 105–150 μm, the SHG response of β-Na₃VOS₃ is 0.61 times
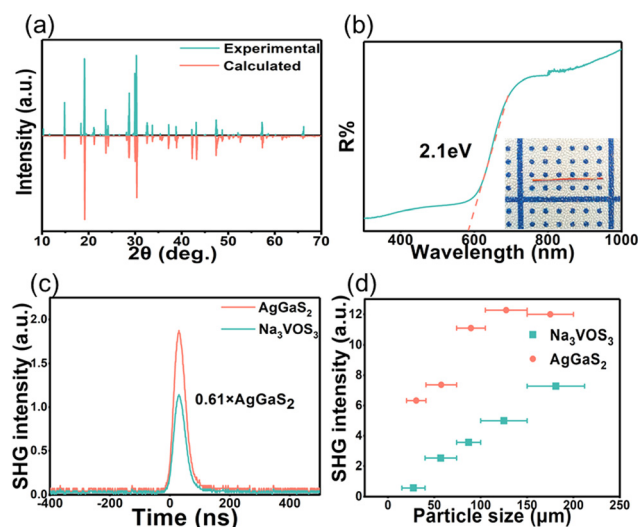
Fig. 3 (a) The experiment powder X-ray diffraction pattern and calculated diffraction pattern of β-Na₃VOS₃; (b) UV-vis/NIR diffuse reflectance spectrum (inset is the photograph of the β-Na₃VOS₃ crystal); (c) the measured SHG signals of β-Na₃VOS₃ and AgGaS₂ (reference) in a particle size range of 100–150 μm; (d) the SHG intensities versus particle sizes with AGS as the references under 2.09 μm irradiation.

that of AgGaS₂, corresponding to a NLO effect of ~7.9 pm V^{-1}, matching well with the calculated result. This value is larger than that for α-Na₃PO₃S (0.2 × SiO₂)[59] and comparable to other NLO oxychalcogenides, like Ba₂SnSi₂O₇S (0.6 × AGS),[60] Sr₂CdGe₂OS₆ (0.6 × AGS),[61] Sr₂ZnSn₂OS₆ (0.7 × AGS),[62]

This journal is © the Partner Organisations 2024

Inorg. Chem. Front., 2024, 11, 5528–5535 | 5531

$BaGeOS_2$ (0.5 × AGS),[63] and $Sr_5Ga_8O_3S_{14}$ (0.8 × AGS).[64] In addition, Raman spectra and photoluminescence (PL) properties were measured and the results are shown in Fig. S2 and S3,† respectively. β-Na_3VOS_3 exhibits four Raman peaks at 216, 419, 454 and 479 cm^{-1}, which can be attributed to the vibrations of the [VOS_3] units, and this compound possesses a wide PL emission with the PL maximum located at 710 nm.

To further investigate the NLO performance of the [VO_xS_{4-x}] (x = 0–4) units with respect to the O/S ratio, we designed a series of $Na_3[VO_xS_{4-x}]$ (x = 0–4) compounds using β-Na_3VOS_3 as the parent structure. In the structures, the O/S positions and their ratio in the tetrahedral [VO_xS_{4-x}] groups are modified. These theoretically optimized structures, as well as their phonon spectra, are shown in Fig. S4 and S5.† The calculated band gaps, NLO coefficients, refractive index and birefringence of the designed compounds are displayed in Table 1 and Fig. 4a. On the basis of the calculated results, two conclusions can be drawn: (i) the positions of the S atoms in the tetrahedra can strongly influence the NLO coefficients. In β-Na_3VOS_3, the S atoms are located at the three bottom corner positions of the tetrahedra, while the O atom is located at

the top corner position along the *c*-axis. As the top corner position is occupied by the S atom in the designed Na_3VOS_3, the maximum SHG coefficient can be increased from d_{15} (10.6 pm V^{-1}) to d_{33} (22.9 pm V^{-1}). (ii) The balanced IR NLO performance is strongly affected by the O/S ratio. A higher ratio results in larger band gaps and smaller NLO coefficients, and *vice versa*. Clearly, the band gap increases from 2.7 eV to 5.6 eV, while the NLO coefficients decrease from 53.5 pm V^{-1} to 5.4 pm V^{-1} as the O/S ratio increases. Such trend is reasonable and consistent with common tendency.[65,66] Notably, all five designed compounds exhibit a large birefringence, verifying the validity of our strategy of using the [VO_xS_{4-x}] tetrahedra to achieve a large birefringence. According to the above discussion, it is clear that the [VO_xS_{4-x}] tetrahedra are good birefringent and NLO active units in the IR region.

The IR transmission is also an important factor for IR NLO applications. Thus, the IR spectra for the five designed compounds were calculated, and the vibrational characteristics of the [VO_xS_{4-x}] (x = 0–4) units were analyzed. It is known that there exists a strong correlation between the wavenumber of the IR absorption and the IR absorption cutoff in a compound.[67,68] With decreasing value of the highest wavenumber, there is a greater red-shift in the IR absorption cutoff. As shown in Fig. 4b, the highest wavenumber IR absorption peak of Na_3VS_4 is close to that of AGS, which indicates its good IR transmission. As O anions are introduced into the structure, the highest wavenumber of IR peaks in $Na_3VO_xS_{4-x}$ (x = 1–4) appear at greater wavenumbers. These peaks can be attributed to the stretching vibration of the V–O bond, indicating the unfavorable role of O atoms in the IR transmission.

Fig. 4 (a) Band gap E_g, largest SHG coefficient d_{ij}(Max), birefringence Δn; (b) IR spectra of Na_3VS_4, Na_3VOS_3, $Na_3VO_2S_2$, Na_3VO_3S, and Na_3VO_4.

Conclusions

We proposed and examined the birefringence enhancing strategy that simultaneously introduces V^{5+} cations and constructs heteroanionic tetrahedra in thiovanadates for the comprehensive IR NLO performance. By this method, the new birefringence record of the pure tetrahedron-based compounds has been increased to 0.37 in $Ba_5V_2O_4S_8$. Combining the theoretical calculations and experimental measurements, the linear and NLO properties of β-Na_3VOS_3, which were highlighted by the systematical theoretical investigation, are reported herein with a strong NLO effect at about 0.6 × AGS, a large birefringence of 0.28, and a wide band gap of about 2.1 eV, indicating its potential for IR NLO applications. Furthermore, the structure–property relationships of β-Na_3VOS_3 and its derivatives were investigated, and they indicate the potential of the [VO_xS_{4-x}] units in enhancing the birefringence and NLO properties. This finding is significant for the development of materials in this system.

Author contributions

Shengzi Zhang: formal analysis, investigation, writing – original draft; Linfeng Dong: formal analysis, investigation,
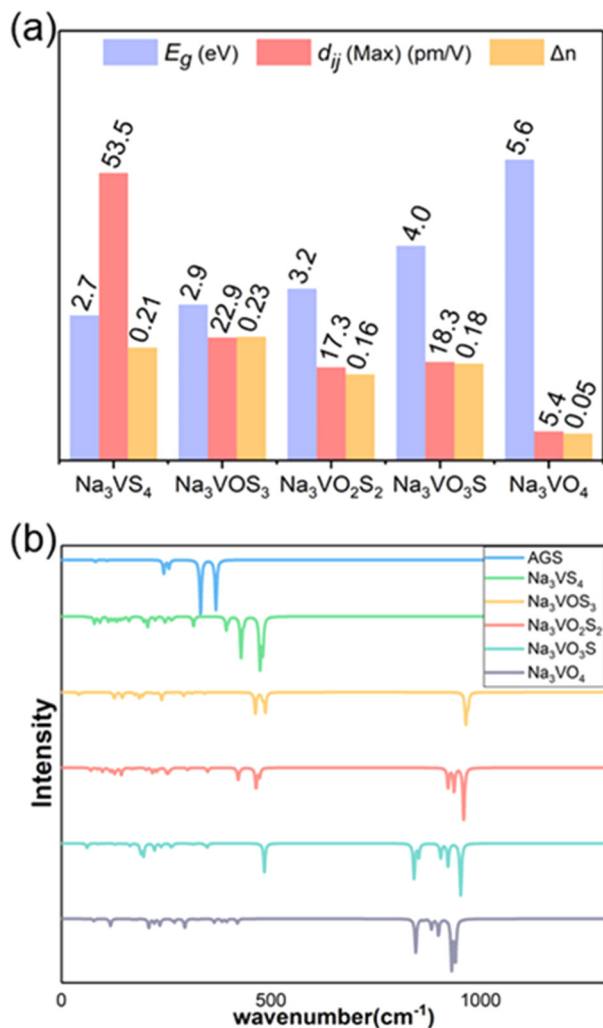
Data availability

The authors confirm that the data supporting the findings of this study are available within the article and its ESI.†

Conflicts of interest

There are no conflicts to declare.

Acknowledgements

References

1 F. Yang, J. Y. Yao, H. Y. Xu, F. F. Zhang, N. X. Zhai, Z. H. Lin, N. Zong, Q. J. Peng, J. Y. Zhang, D. F. Cui, Y. C. Wu, C. T. Chen and Z. Y. Xu, Midinfrared Optical Parametric Amplifier With 6.4–11 μm Range Based on $BaGa_4Se_7$, *IEEE Photonics Technol. Lett.*, 2015, **27**, 1100–1103.

2 W. Chen, E. Poullet, J. Burie, D. Boucher, M. W. Sigrist, J.-J. Zondy, L. Isaenko, A. Yèlisseyev and S. Lobanov, Widely tunable continuous-wave mid-infrared radiation (5.5–11 μm) by difference-frequency generation in $LiInS_2$ crystal, *Appl. Opt.*, 2005, **44**, 4123–4129.

3 S. Ehret and H. Schneider, Generation of subpicosecond infrared pulses tunable between 5.2 μm and 18 μm at a repetition rate of 76 MHz, *Appl. Phys. B*, 1998, **66**, 27–30.

4 W. Shi and Y. J. Ding, A monochromatic and high-power terahertz source tunable in the ranges of 2.7–38.4 and 58.2–3540 μm for variety of potential applications, *Appl. Phys. Lett.*, 2004, **84**, 1635–1637.

5 G. D. Boyd, K. Nassau, R. C. Miller, W. L. Bond and A. Savage, $LiNbO_3$: an efficient phase matchable nonlinear optical material, *Appl. Phys. Lett.*, 1964, **5**, 234–236.

6 C. T. Chen, Y. C. Wu, A. D. Jiang, B. C. Wu, G. M. You, R. K. Li and S. J. Lin, New Nonlinear Optical Crystal LiB_3O_5, *J. Opt. Soc. Am. B*, 1989, **6**, 616–621.

7 D. F. Eaton, Nonlinear Optical Materials, *Science*, 1991, **253**, 281–287.

8 M. Pushkarsky, A. Tsekoun, I. Dunayevskiy, R. Go and C. Patel, Sub-parts-per-billion level detection of NO_2 using room-temperature quantum cascade lasers, *Proc. Natl. Acad. Sci. U. S. A.*, 2006, **103**, 10846–10849.

9 M. B. Pushkarsky, I. G. Dunayevskiy, M. Prasanna, A. G. Tsekoun, R. Go and C. K. Patel, High-sensitivity detection of TNT, *Proc. Natl. Acad. Sci. U. S. A.*, 2006, **103**, 19630–19634.

10 U. Willer, M. Saraji, A. Khorsandi, P. Geiser and W. Schade, Near- and mid-infrared laser monitoring of industrial processes, environment and security applications, *Opt. Laser Eng.*, 2006, **44**, 699–710.

11 A. Mukherjee, I. Dunayevskiy, M. Prasanna, R. Go and C. K. N. Patel, Sub-parts-per-billion level detection of dimethyl methyl phosphonate (DMMP) by quantum cascade laser photoacoustic spectroscopy, *Appl. Opt.*, 2008, **47**, 1543–1548.

12 D. Pestov, X. Wang, G. O. Ariunbold, R. K. Murawski, V. A. Sautenkov, A. Dogariu, A. V. Sokolov and M. O. Scully, Single-shot detection of bacterial endospores via coherent Raman spectroscopy, *Proc. Natl. Acad. Sci. U. S. A.*, 2008, **105**(2), 422–427.

13 I. Chung, J.-H. Song, J. I. Jang, A. J. Freeman, J. B. Ketterson and M. G. Kanatzidis, Flexible Polar Nanowires of $Cs_5BiP_4Se_{12}$ from Weak Interactions between Coordination Complexes: Strong Nonlinear Optical Second Harmonic Generation, *J. Am. Chem. Soc.*, 2009, **131**, 2647–2656.

14 L. Kang, D. M. Ramo, Z. Lin, P. D. Bristowe, J. Qin and C. Chen, First principles selection and design of mid-IR nonlinear optical halide crystals, *J. Mater. Chem. C*, 2013, **1**, 7363–7370.

15 L. Kang, M. Zhou, J. Yao, Z. Lin, Y. Wu and C. Chen, Metal Thiophosphates with Good Mid-infrared Nonlinear Optical Performances: A First-Principles Prediction and Analysis, *J. Am. Chem. Soc.*, 2015, **137**, 13049–13059.

16 A. Harasaki and K. Kato, New Data on the Nonlinear Optical Constant, Phase-Matching, and Optical Damage of $AgGaS_2$, *Jpn. J. Appl. Phys.*, 1997, **36**, 700.

17 G. Boyd, H. Kasper, J. McFee and F. Storz, Linear and nonlinear optical properties of some ternary selenides, *IEEE J. Quantum Electron.*, 1972, **8**, 900–908.

18 G. Boyd, E. Buehler and F. Storz, Linear and nonlinear optical properties of $ZnGeP_2$ and CdSe, *Appl. Phys. Lett.*, 1971, **18**, 301–304.

19 J. Y. Yao, D. J. Mei, L. Bai, Z. S. Lin, W. L. Yin, P. Z. Fu and Y. C. Wu, $BaGa_4Se_7$: A New Congruent-Melting IR Nonlinear Optical Material, *Inorg. Chem.*, 2010, **49**, 9212–9216.

20 L. Isaenko, A. Yelisseyev, S. Lobanov, A. Titov, V. Petrov, J.-J. Zondy, P. Krinitsin, A. Merkulov, V. Vedenyapin and J. Smirnova, Growth and properties of $LiGaX_2$ (X = S, Se, Te) single crystals for nonlinear optical applications in the mid-IR, *Cryst. Res. Technol.*, 2003, **38**, 379–387.

21 L. Isaenko, I. Vasilyeva, A. Merkulov, A. Yelisseyev and S. Lobanov, Growth of new nonlinear crystals $LiMX_2$ (M = Al, In, Ga; X = S, Se, Te) for the mid-IR optics, *J. Cryst. Growth*, 2005, **275**, 217–223.

This journal is © the Partner Organisations 2024

Inorg. Chem. Front., 2024, **11**, 5528–5535 | **5533**

22 K. T. Zawilski, P. G. Schunemann, T. C. Pollak, D. E. Zelmon, N. C. Fernelius and F. Kenneth Hopkins, Growth and characterization of large $CdSiP_2$ single crystals, *J. Cryst. Growth*, 2010, **312**, 1127–1132.

23 W.-F. Chen, X.-M. Jiang, B.-W. Liu and G.-C. Guo, Wide band gaps in nonlinear optical materials $AMgAgGa_6S_{11}$ (A = K, Rb) achieved by the incorporation of dual s-block elements in Ag-based sulfide, *Mater. Today Phys.*, 2023, **37**, 101199.

24 H. Wang, X. Pan, W. Zhao, Y. Chu and J. Li, A New Infrared Nonlinear Optical Material $BaZnGeS_4$ with Wide Band Gap and Large Nonlinear Optical Response, *Inorg. Chem. Front.*, 2023, **10**, 6253–6261.

25 X. Zhao, C. Lin, J. Chen, M. Luo, F. Xu, S. Yang, S. Shi, B. Li and N. Ye, Halonitrides Zn_2NX (X = Cl, Br): Novel Mid-Infrared Nonlinear Optical Materials, *Chem. Mater.*, 2021, **33**, 1462–1470.

26 J. Xu, H. Wu, H. Yu, W. Zhang, Z. Hu, J. Wang, Y. Wu and P. S. Halasyamani, $Li_2K_4TiOGe_4O_{12}$: A Stable Mid-Infrared Nonlinear Optical Material, *Chem. Mater.*, 2020, **32**, 906–912.

27 D. Mei, W. Cao, N. Wang, X. Jiang, J. Zhao, W. Wang, J. Dang, S. Zhang, Y. Wu, P. Rao and Z. Lin, Breaking through the "3.0 eV wall" of energy band gap in mid-infrared nonlinear optical rare earth chalcogenides by charge-transfer engineering, *Mater. Horiz.*, 2021, **8**, 2330–2334.

28 Y. Chu, H. Wang, Q. Chen, X. Su, Z. Chen, Z. Yang, J. Li and S. Pan, "Three-in-One": A New Hg-Based Selenide $Hg_7P_2Se_{12}$ Exhibiting Wide Infrared Transparency Range and Strong Nonlinear Optical Effect, *Adv. Funct. Mater.*, 2024, 2314933.

29 F. Liang, L. Kang, Z. Lin and Y. Wu, Mid-Infrared Nonlinear Optical Materials Based on Metal Chalcogenides: Structure–Property Relationship, *Cryst. Growth Des.*, 2017, **17**, 2254–2289.

30 P. Gong, F. Liang, L. Kang, X. Chen, J. Qin, Y. Wu and Z. Lin, Recent advances and future perspectives on infrared nonlinear optical metal halides, *Coord. Chem. Rev.*, 2019, **380**, 83–102.

31 A. Abudurusuli, J. Huang, P. Wang, Z. Yang, S. Pan and J. Li, $Li_4MgGe_2S_7$: The First Alkali and Alkaline-Earth Diamond-Like Infrared Nonlinear Optical Material with Exceptional Large Band Gap, *Angew. Chem., Int. Ed.*, 2021, **60**, 24131–24136.

32 K. Wu, B. Zhang, Z. Yang and S. Pan, New Compressed Chalcopyrite-like $Li_2BaMIVQ_4$ (MIV = Ge, Sn; Q = S, Se): Promising Infrared Nonlinear Optical Materials, *J. Am. Chem. Soc.*, 2017, **139**, 14885–14888.

33 F. Liang, L. Kang, Z. Lin, Y. Wu and C. Chen, Analysis and prediction of mid-IR nonlinear optical metal sulfides with diamond-like structures, *Coord. Chem. Rev.*, 2017, **333**, 57–70.

34 M. Chen, H. Xue and S. Guo, Multinary metal chalcogenides with tetrahedral structures for second-order nonlinear optical, photocatalytic, and photovoltaic applications, *Coord. Chem. Rev.*, 2018, **368**, 115–133.

35 P. Gong, F. Liang, L. Kang and Z. Lin, Mid-Infrared Nonlinear Optical Halides with Diamond-like Structures: A Theoretical and Experimental Study, *Chem. Mater.*, 2022, **34**, 5301–5310.

36 H. Lin, L. Chen, L.-J. Zhou and L.-M. Wu, Functionalization Based on the Substitutional Flexibility: Strong Middle IR Nonlinear Optical Selenides $AX^{II}_4X^{III}_5Se_{12}$, *J. Am. Chem. Soc.*, 2013, **135**, 12914–12921.

37 J. Chen, C. Lin, D. Zhao, M. Luo, G. Peng, B. Li, S. Yang, Y. Sun and N. Ye, Anionic Aliovalent Substitution from Structure Models of ZnS: Novel Defect Diamond-like Halopnictide Infrared Nonlinear Optical Materials with Wide Band Gaps and Large SHG Effects, *Angew. Chem., Int. Ed.*, 2020, **59**, 23549–23553.

38 K. M. Ok, P. S. Halasyamani, D. Casanova, M. Llunell, P. Alemany and S. Alvarez, Distortions in Octahedrally Coordinated d^0 Transition Metal Oxides: A Continuous Symmetry Measures Approach, *Chem. Mater.*, 2006, **18**, 3176–3183.

39 Z. Xie, S. Cheng, S. Li and H. Ding, $NaCa_4V_5O_{17}$ with isolated V_2O_7 dimer and V_3O_{10} trimer exhibiting a large birefringence, *J. Solid State Chem.*, 2019, **269**, 94–99.

40 H. T. Luo, T. Tkaczyk, E. L. Dereniak, K. Oka and R. Sampson, High birefringence of the yttrium vanadate crystal in the middle wavelength infrared, *Opt. Lett.*, 2006, **31**, 616–618.

41 X. Liu, Y.-C. Yang, M.-Y. Li, L. Chen and L.-M. Wu, Anisotropic structure building unit involving diverse chemical bonds: a new opportunity for high-performance second-order NLO materials, *Chem. Soc. Rev.*, 2023, **52**, 8699–8720.

42 B. Zhang, G. Han, Y. Wang, X. Chen, Z. Yang and S. Pan, Expanding Frontiers of Ultraviolet Nonlinear Optical Materials with Fluorophosphates, *Chem. Mater.*, 2018, **30**, 5397–5403.

43 J. Lu, J.-N. Yue, L. Xiong, W.-K. Zhang, L. Chen and L.-M. Wu, Uniform Alignment of Non-π-Conjugated Species Enhances Deep Ultraviolet Optical Nonlinearity, *J. Am. Chem. Soc.*, 2019, **141**, 8093–8097.

44 M. Luo, C. Lin, D. Lin and N. Ye, Rational Design of the Metal-Free $KBe_2BO_3F_2$-(KBBF) Family Member $C(NH_2)_3SO_3F$ with Ultraviolet Optical Nonlinearity, *Angew. Chem., Int. Ed.*, 2020, **59**, 15978–15981.

45 H. Fan, N. Ye and M. Luo, New Functional Groups Design toward High Performance Ultraviolet Nonlinear Optical Materials, *Acc. Chem. Res.*, 2023, **56**, 3099–3109.

46 B. Xu, P. Gong, F. Liu, X. Zhang, H. Huo and Z. Lin, $(SO_3CF_3)^-$: A Non-π-Conjugated Motif for Nonlinear Optical Crystals Transparent into the Deep-Ultraviolet Region, *Adv. Opt. Mater.*, 2023, 2301725.

47 X. Zhang, L. Kang, P. Gong, Z. Lin and Y. Wu, Nonlinear Optical Oxythiophosphate Approaching the Good Balance with Wide Ultraviolet Transparency, Strong Second Harmonic Effect, and Large Birefringence, *Angew. Chem., Int. Ed.*, 2021, **60**, 6386–6390.

5534 | *Inorg. Chem. Front.*, 2024, **11**, 5528–5535

This journal is © the Partner Organisations 2024

48 R. Wang, F. Liang, F. Wang, Y. Guo, X. Zhang, Y. Xiao, K. Bu, Z. Lin, J. Yao, T. Zhai and F. Huang, $Sr_6Cd_2Sb_6O_7S_{10}$: Strong SHG Response Activated by Highly Polarizable Sb/O/S Groups, *Angew. Chem.*, 2019, **131**, 8162–8165.

49 B.-W. Liu, X.-M. Jiang, G.-E. Wang, H.-Y. Zeng, M.-J. Zhang, S.-F. Li, W.-H. Guo and G.-C. Guo, Oxychalcogenide $BaGeOSe_2$: highly distorted mixed-anion building units leading to a large second-harmonic generation response, *Chem. Mater.*, 2015, **27**, 8189–8192.

50 P. Gong, F. Liang, L. Kang and Z. Lin, Mid-Infrared Nonlinear Optical Halides with Diamond-like Structures: A Theoretical and Experimental Study, *Chem. Mater.*, 2022, **34**, 5301–5310.

51 S. Chen, D. Huang, P. Xu, X. Gong, W. Xue, L. Lei, R. Deng, J. Li and Z. Li, Facet-Engineered Surface and Interface Design of Monoclinic Scheelite Bismuth Vanadate for Enhanced Photocatalytic Performance, *ACS Catal.*, 2020, **10**, 1024–1059.

52 S. Liu, X. Liu, S. Zhao, Y. Liu, L. Li, Q. Ding, Y. Li, Z. Lin, J. Luo and M. Hong, An Exceptional Peroxide Birefringent Material Resulting from d–π Interactions, *Angew. Chem., Int. Ed.*, 2020, **59**, 9414–9417.

53 H. Hosseini and S. Shahrokhian, Advanced binder-free electrode based on core–shell nanostructures of mesoporous $Co_3V_2O_8$-$Ni_3V_2O_8$ thin layers@porous carbon nanofibers for high-performance and flexible all-solid-state supercapacitors, *Chem. Eng. J.*, 2018, **341**, 10–26.

54 L. Dong, S. Zhang, P. Gong, L. Kang and Z. Lin, Evaluation and prospect of Mid-Infrared nonlinear optical materials in f^0 rare earth (RE = Sc, Y, La) chalcogenides, *Coord. Chem. Rev.*, 2024, **509**, 215805.

55 B. Almoussawi, M. Huvé, V. Dupray, S. Clevers, V. Duffort, O. Mentré, P. Roussel, A. M. Arevalo-Lopez and H. Kabbour, Oxysulfide $Ba_5(VO_2S_2)_2(S_2)_2$ Combining Disulfide Channels and Mixed-Anion Tetrahedra and Its Third-Harmonic-Generation Properties, *Inorg. Chem.*, 2020, **59**, 5907–5917.

56 S. Nicoud, O. Mentré and H. Kabbour, The $Ba_{10}S(VO_3S)_6$ Oxysulfide: One-Dimensional Structure and Mixed Anion Chemical Bonding, *Inorg. Chem.*, 2019, **58**, 1349–1357.

57 S. Schnabel and C. Roehr, Mixed thio/oxo orthovanadates $Na_3[VS_xO_{4-x}]$ (x = 2, 3): Synthesis-crystal structures-properties, *Z. Naturforsch., B: Chem. Sci.*, 2005, **60**, 479–490.

58 S. Kurtz and T. Perry, A powder technique for the evaluation of nonlinear optical materials, *J. Appl. Phys.*, 1968, **39**, 3798–3813.

59 N. J. Takas and J. A. Aitken, Phase Transitions and Second-Harmonic Generation in Sodium Monothiophosphate, *Inorg. Chem.*, 2006, **45**, 2779–2781.

60 Y.-F. Shi, Z. Ma, B.-X. Li, X.-T. Wu, H. Lin and Q.-L. Zhu, Phase matching achieved by isomorphous substitution in IR nonlinear optical material $Ba_2SnSSi_2O_7$ with an undiscovered $[SnO_4S]$ functional motif, *Mater. Chem. Front.*, 2022, **6**, 3054–3061.

61 M.-Y. Ran, S.-H. Zhou, B. Li, W. Wei, X.-T. Wu, H. Lin and Q.-L. Zhu, Enhanced Second-Harmonic-Generation Efficiency and Birefringence in Melillite Oxychalcogenides $Sr_2MGe_2OS_6$ (M = Mn, Zn, and Cd), *Chem. Mater.*, 2022, **34**, 3853–3861.

62 Y. Cheng, H. Wu, H. Yu, Z. Hu, J. Wang and Y. Wu, Rational design of a promising oxychalcogenide infrared nonlinear optical crystal, *Chem. Sci.*, 2022, **13**, 5305–5310.

63 X. Zhang, Y. Xiao, R. Wang, P. Fu, C. Zheng and F. Huang, Synthesis, crystal structures and optical properties of non-centrosymmetric oxysulfides $AeGeS_2O$ (Ae = Sr, Ba), *Dalton Trans.*, 2019, **48**, 14662–14668.

64 R. Wang, Y. Guo, X. Zhang, Y. Xiao, J. Yao and F. Huang, $Sr_5Ga_8O_3S_{14}$: A Nonlinear Optical Oxysulfide with Melilite-Derived Structure and Wide Band Gap, *Inorg. Chem.*, 2020, **59**, 9944–9950.

65 J. j. Xu and K. Wu, Comprehensive review on multiple mixed-anion ligands, physicochemical performances and application prospects in metal oxysulfides, *Coord. Chem. Rev.*, 2023, **486**, 215139.

66 M.-Y. Ran, A. Y. Wang, W.-B. Wei, X.-T. Wu, H. Lin and Q.-L. Zhu, Recent progress in the design of IR nonlinear optical materials by partial chemical substitution: Structural evolution and performance optimization, *Coord. Chem. Rev.*, 2023, **481**, 215059.

67 K. Wu, J. Li, C. Lin, C. Mang and B. Zhuang, Infrared absorption-edges of molecular nonlinear optical crystals: an ab initio calculation, *Appl. Phys. A*, 2003, **76**, 427–431.

68 K.-c. Wu and J. Li, Infrared Absorption Cut-Off of Molecular Nonlinear Optical Crystals: Theoretical Studies on Vibrational Spectra of MDNB, Urea and MNA Molecules, *Chin. Phys. Lett.*, 1999, **16**, 925–927.

This journal is © the Partner Organisations 2024

Inorg. Chem. Front., 2024, **11**, 5528–5535 | **5535**